NAP-2015

Simulation of Reciprocal Space Maps for Thin Ion-Implanted Layers in Yttrium-Iron Garnet Films with Defects

S.I. Olikhovskii[1,*], O.S. Skakunova[1], V.B. Molodkin[1], E. G. Len'[1], B.K. Ostafiychuk[2], V.M. Pylypiv[2]

[1] *G.V. Kurdyumov Institute for Metal Physics of NASU, Vernadsky Blvd. 36, 03680 Kyiv, Ukraine*
[2] *V. Stefanyk Precarphatian National University, Shevchenko Str. 57, 76025 Ivano-Frankivsk, Ukraine*

Numerical simulation of the reciprocal space maps measured from the ion-implanted single-crystal yttrium-iron garnet films on gadolinium-gallium garnet substrate has been carried out basing on the theoretical model of the triple-crystal dynamical diffractometry of crystalline multilayer systems with inhomogeneous strain distributions and randomly distributed defects. The presence of growth defects in both film and substrate as well as radiation defects created in subsurface layer of nanometer-scale thickness after 90 keV F^+ ion implantation was taken into account in the proposed model of the film system.

Keywords: X-Ray Dynamical Diffraction Theory, Yttrium Iron Garnet, Film, Ion Implantation, Strain, Radiation Defects.

1. INTRODUCTION

Modern technologies allow to grow almost perfect multilayered crystalline systems and purposefully to influence on their physical properties by the controlled introducing different structural defects. In particular, epitaxial single-crystal yttrium iron garnet (YIG) $Y_3Fe_5O_{12}$ films grown on gadolinium gallium garnet (GGG) $Gd_3Ga_5O_{12}$ substrate are widely used in energy-independent magnetic memory devices, magnetic microelectronics, and integral magneto-optics, etc. (see, e.g., Ref. [1]). Modification of physical properties of their functional layers, the sizes of which often are of nanometer scale, is carried out, in particular, by ion implantation.

X-ray diffraction methods are most widely used to characterize structural defects and strains in the modified crystal layers, In particular, the measurements by high-resolution triple-crystal diffractometer (TCD) were carried out to characterize inhomogeneous strain distributions and structure imperfections in implanted garnet crystals [2, 3]. These methods are highly informative if the analytical formulas which give the adequate description of measured diffraction intensity distributions are available.

The purpose of this work is demonstration of diagnostic possibilities offered by the theoretical method for interpretation of results of high-resolution X-ray diffraction mapping the real film and multilayered systems with defects [4]. This method of structural diagnostics will be applied to the simulation of the influence of nanometer-sized defects and inhomogeneous strain distributions in the epitaxial YIG films grown on GGG substrate, which were implanted with 90 keV F^+ ions, on the form of coherent and diffuse components of diffraction intensity distributions on reciprocal lattice maps measured by TCD.

2. COHERENT AND DIFFUSE COMPONENTS OF RECIPROCAL LATTICE MAPS

Differential X-ray diffraction intensity distributions measured by TCD from crystalline multilayer systems with inhomogeneous strain distributions and randomly distributed defects can be represented as a sum of coherent (I_{coh}) and diffuse (I_{diff}) components.

If Bragg angles for monochromator, analyzer, and crystal under investigation are nearly equal, it is possible to ignore the dispersion effects and the coherent component of the two-dimensional intensity distribution can be calculated approximately in the case of quasi-non-dispersive geometry ($m, -n, m$) as follows [5, 6]:

$$I_{coh}\left(\Delta\theta, \Delta\theta'\right) \approx I_0 b_S \int_{-x_m}^{x_m} dz R_M\left(b_M^{-1}z\right) R_{coh}\left(z + \Delta\theta\right) \times$$
$$\times R_A\left[b_S z + \Delta\theta\left(1 + b_S\right) - \Delta\theta'\right], \quad (1)$$

where I_0 is an intensity of incident X-ray beam, R_M and R_A are the reflection coefficients of monochromator and analyzer crystals, $\Delta\theta$ and $\Delta\theta'$ are the angular deviations of the crystal under investigation and analyzer crystal, b_M and b_S are asymmetry parameters of monochromator and sample crystals, respectively. The expression for the coherent component of the reflection coefficient $R_{coh}(\Delta\theta)$ for imperfect crystal has been derived elsewhere earlier [7] and takes into account all the dynamical scattering effects including the extinction of Bragg waves due to diffuse scattering by defects.

Particularly, the dynamical consideration is necessary in the case of X-ray diffraction by the implanted YIG films, thickness of which is of the order of an extinction length. The coherent component of reflection coefficient of such inhomogeneous crystalline system with chaotically distributed defects can be calculated in so called 'layer approximation' by using the recurrence relations between coherent components of amplitude

---
[*] olikhovsky@meta.ua

reflection coefficients of adjacent layers for Bragg diffraction geometry [5]:

$$R_j = \frac{r_j + R_{j-1}(t_j^2 - \zeta_j r_j^2)}{1 - \zeta_j r_j R_{j-1}}, \qquad (2)$$

where r_j and t_j are amplitude reflectivity and transmissivity of j th layer, respectively, and $\zeta_j \approx 1$.

The diffuse component of the diffraction intensity measured by TCD can be represented approximately by the following expression [5, 6]:

$$I_{\text{diff}}(\Delta\theta, \Delta\theta') \approx I_0 R_{i\text{M}} R_{i\text{A}} r_{\text{diff}}(\mathbf{\kappa}). \qquad (3)$$

where $R_{i\text{M}}$ and $R_{i\text{A}}$ are the integrated reflectivities of monochromator and analyzer crystals, respectively, and components k_x and k_z of two-dimensional vector $\mathbf{\kappa}$ describe a deviation from the reciprocal lattice point H in the coherent scattering plane.

Function $r_{\text{diff}}(\mathbf{\kappa})$ in Eq. (3) represents the diffuse component of the differential reflection coefficient of the investigated sample after integration over vertical divergence [7]:

$$r_{\text{diff}}(\mathbf{\kappa}) = \sum_{j=0}^{M} F_{\text{ext}}^j F_{\text{abs}}^j r_{\text{diff}}^j(\mathbf{\kappa}), \qquad (4)$$

where F_{ext}^j is the extinction factor describing the influence of redistribution of X-ray intensity between transmitted and diffracted coherent waves in j th layer, the factor F_{abs}^j describes photoelectric absorption and absorption due to diffuse scattering in layers lying above j th layer, and $r_{\text{diff}}^j(\mathbf{\kappa})$ is the diffuse component of the differential reflection coefficient of j th layer.

Thus, the formulas presented above provide the possibility for the effective, i.e., with minimization of required calculation time expenses, and quantitative self-consistent analysis of coherent and diffuse components of reciprocal lattice maps, which are measured from crystalline film or multilayer systems, including those with inhomogeneous strain distributions, large strain gradients at layer interfaces, and randomly distributed defects of different types in all the layers and substrate.

3. MODEL OF THE DEFECT STRUCTURE IN ION-IMPLANTED YIG FILM

The sample of the epitaxial YIG film with 5.33 μm thickness, which was grown on GGG substrate and implanted with F+ ions of the energy of 90 keV at dose $D = 6 \cdot 10^{13}$ cm^{-2}, has been chosen as a model object for simulation.

This sample was investigated earlier by using the high-resolution double-crystal X-ray diffractometer [8]. As has been established by simultaneous treatment of the rocking curves measured for two reflections, the strain profile in YIG film implanted with F+ ions has the shape shown in Fig. 1. This strain profile is formed due to the radiation defects, which are distributed inhomogeneously in depth and cause the corresponding «in average» inhomogeneous strain. The depth profile of the strain caused by ion implantation was calculated by

using the determined characteristics of spherical amorphous clusters in implanted layer, namely, concentration of $5 \cdot 10^{20}$ cm^{-3}, radius of 0.75 nm, and volume misfit strain at the boundary between cluster and crystal matrix of 0.0375.
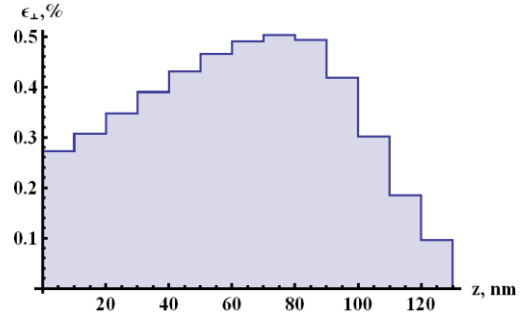

Fig. 1 – Strain profile in YIG film implanted with F+ ions ($E = 90$ keV) at dose $D = 6 \cdot 10^{13}$ cm^{-2}

Besides, in the model of defect structure of the implanted epitaxial single-crystalline system of YIG film grown on GGG substrate the presence of two types of growth microdefects, namely, spherical clusters and circular prismatic dislocation loops was taken into account. Their characteristics were supposed to be the same as determined in Ref. [8], namely, for spherical clusters in YIG film and GGG substrate we putted cluster radii of 10 and 8 nm, respectively, concentration of 10^{14} cm^{-3}, and volume misfit strain at the boundary between cluster and crystal matrix of 0.03. Similarly, for dislocation loops of <110>-type in YIG film we putted dislocation loop radius of 5 nm and concentration of 10^{15} cm^{-3}, whereas in GGG substrate we putted dislocation loop radii of 5 and 90 nm, and concentrations of 10^{15} and $1,2 \cdot 10^{12}$ cm^{-3}, respectively.

The YIG/GGG film system in whole was considered as a multilayer system in each layer of which the strain was consisted of sum of average and fluctuating components. At modeling the average strain distribution, the implanted layer was subdivided into 10 nm thick laminae, whereas the transition layer between film and substrate was subdivided into layers with thicknesses of order of few hundreds of nanometers.

4. SIMULATION OF RECIPROCAL LATTICE MAPS FOR ION-IMPLANTED YIG FILMS WITH DEFECTS

The results of numeral simulation of reciprocal lattice maps are described below for the YIG film, which was implanted with F+ ions of the energy of 90 keV at dose $D = 6 \cdot 10^{13}$ cm^{-2}. The maps were simulated for the case of measurements by the high-resolution PANalytical X`Pert Pro MRD XL diffractometer for (444) reflection of characteristic Cu$K_{\alpha 1}$ radiation in the symmetrical Bragg diffraction geometry at the sample under investigation. As far as the Bragg angle for Ge (220) reflection used in monochromator and analyzer crystals of the diffractometer is nearly equal to Bragg angles for (444) reflection of YIG film and GGG substrate, the influence of dispersion effects can be neglected and for the calculation of coherent and diffuse components of reciprocal lattice maps the simplified formulas (1) and (3) can be used.

To elucidate the role of growth microdefects in YIG film and GGG substrate in the formation of diffraction patterns, we first calculated the reciprocal lattice map for the symmetrical 444 reflection of $CuK_{\alpha 1}$ radiation from as-grown YIG/GGG film system (Fig. 2). As is evident from comparison between the total reciprocal lattice map and its coherent component, the diffuse scattering intensity from microdefects in both YIG film and GGG substrate give a substantial contribution to the formation of observed diffraction intensity distributions.
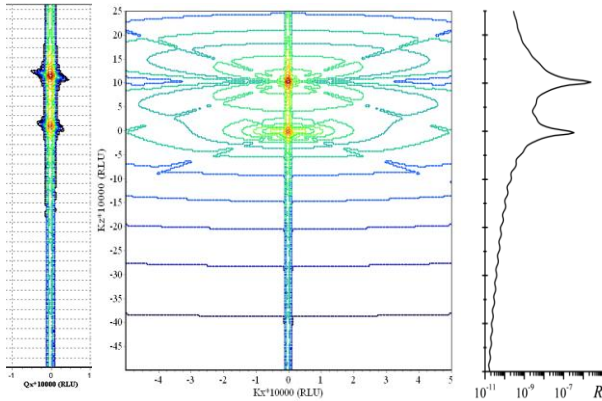

Fig. 2 – Reciprocal lattice map (middle), its coherent component (left), and longitudinal cross section (right) for 444 reflection of $CuK_{\alpha 1}$ radiation from as-grown YIG/GGG film system

The reciprocal lattice map simulated for the symmetrical 444 reflection of $CuK_{\alpha 1}$ radiation from the YIG/GGG film system implanted with F^+ ions of 90 keV energy at dose $D = 6 \cdot 10^{13}$ cm^{-2} is shown in Fig. 3.
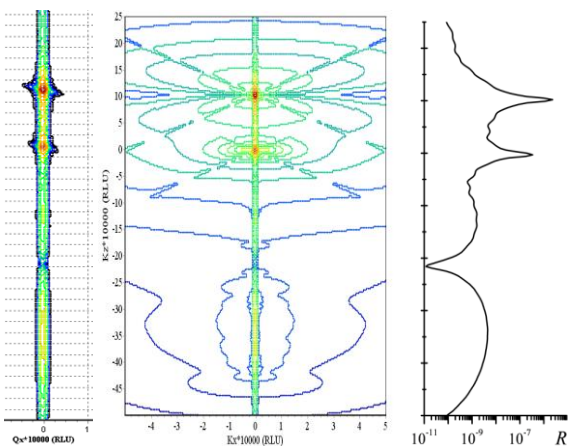

Fig. 3 – Reciprocal lattice map (middle), its coherent component (left), and longitudinal cross section (right) for 444 reflection of $CuK_{\alpha 1}$ radiation from YIG/GGG film system implanted with F^+ ions (E = 90 keV) at dose $D = 6 \cdot 10^{13}$ cm^{-2}

As can be seen by comparing Figs. 2 and 3, the irregularly shaped diffuse scattering intensity distribution from spherical clusters in implanted YIG layer appears additionally to the diffuse scattering intensity distributions from microdefects in both YIG film and GGG substrate around corresponding reciprocal lattice points. It should be remarked that the irregular shape of diffuse scattering intensity distribution from spherical clusters in implanted layer is caused by the inhomogeneous 'in-average' strain distribution in this layer, which leads to smoothing and deformation of the double-drop form known for isodiffuse lines from spherical clusters.

It should be emphasized especially that longitudinal cross sections of the simulated reciprocal lattice maps in Figs. 2 and 3 closely coincide in form with the rocking curves, which were measured by using the high-resolution double-crystal X-ray diffractometer for the corresponding as-grown and implanted epitaxial YIG films [8]. Only the distinction consists in that the oscillations at the tail of the rocking curve measured from implanted epitaxial YIG film are something smoothed as compared with longitudinal cross section of the simulated reciprocal lattice map in Fig. 3 what is explained by an additional contribution of diffuse scattering intensity from defects in implanted YIG layer due to integration over vertical divergence.

5. RESUME AND CONCLUSIONS

On the basis of the created theoretical model of the triple-crystal X-ray dynamical diffractometry of the multilayered crystalline systems with inhomogeneous strain profile and randomly distributed defects, the numeral simulation of reciprocal lattice maps which are measured from the ion-implanted single-crystal YIG films on GGG substrate has been carried out. The presence of growth defects in both film and substrate as well as radiation defects created in subsurface layer was taken into account

It is established that, as a result of superposition of coherent and diffuse scattering intensities from defects of various types in different layers with heterogeneous strain, the reciprocal lattice maps take the form which substantially differs from that characteristic for crystals with homogeneous strain and one type of defects.

Self-consistent description of coherent and diffuse components of dynamical X-ray scattering with account for instrumental factors of TCD allows the correct quantitative analysis of complete reciprocal lattice maps measured from inhomogeneous imperfect crystal structures with defects.

REFERENCES

1. T. Wehlus, T. Körner, S. Leitenmeier, A. Heinrich, B. Stritzker, *phys. status solidi a* **208**, 252 (2011).
2. B.K. Ostafiychuk, I.P. Yaremiy, S.I. Yaremiy, V. D. Fedoriv, U.O. Tomyn, M.M. Umantsiva, I.M. Fodchuk, V.P. Kladko, *Cryst. Rep.* **58**, 1017 (2013).
3. I.M. Fodchuk, V.V. Dovganiuk, I.I. Gutsuliak, I.P. Yaremiy, A.Y. Bonchyk, G.V. Savytsky, I.M. Syvorotka, O.S. Skakunova, *Metallofiz. Noveishie Tekhnol.* **35**, 1209 (2013).
4. O.S. Skakunova, S.I. Olikhovskii, V.B. Molodkin, E.G. Len, E.M. Kislovskii, O.V. Reshetnyk, T.P. Vladimirova, E.V. Kochelab, V.V. Lizunov, S.V. Lizunova, V.L. Makivs'ka, M.G. Tolmachov, L.M. Skapa, Ya.V. Vasylyk, K.V. Fuzik, *Metallofiz. Noveishie Tekhnol.* **37**, 409 (2015).
5. V.B. Molodkin, S.I. Olikhovskii, E.G. Len, E.N. Kislovskii, V.P. Kladko, O.V. Reshetnyk, T.P. Vladimirova, B.V. Sheludchenko, *phys. status solidi a* **206**, 1761 (2009).
6. E.N. Kislovskii, V.B. Molodkin, S.I. Olikhovskii, E.G. Len, B.V. Sheludchenko, S.V. Lizunova, T.P. Vladimirova, E.V. Kochelab, O.V. Reshetnik, V.V. Dovganyuk, I.M. Fodchuk, T.V. Litvinchuk, V.P. Klad'ko, *Journal of Surface Investigation. X-Ray, Synchrotron and Neutron Techniques* **7**, 523 (2013).
7. V.B. Molodkin, S.I. Olikhovskii, Ye.M. Kyslovskyy, I.M. Fodchuk, E.S. Skakunova, E.V. Pervak , V.V. Molodkin, *phys. status solidi a* **204**, 2606 (2007).
8. S.I. Olikhovskii, O.S. Skakunova, V.B. Molodkin, V.V. Lizunov, Ye.M. Kyslovs'kyy, T.P. Vladimirova, O.V. Reshetnyk, V.M. Pylypiv, V.O. Kotsyubynsky, B.K. Ostafiychuk, I.P. Yaremiy, O.Z. Garpul', *Proc. NAP* **3**, 01PCSI10 (2014).